NASA TECHNICAL MEMORANDUM

NASA TM X-73,157

NASA TM X- 73,157

AN EXPERIMENTAL AND COMPUTATIONAL INVESTIGATION OF THE FLOW FIELD ABOUT A TRANSONIC AIRFOIL IN SUPERCRITICAL FLOW WITH TURBULENT BOUNDARY-LAYER SEPARATION

Morris W. Rubesin, Arthur F. Okuno, Lionel L. Levy, Jr.,
John B. McDevitt, and H. Lee Seegmiller

Ames Research Center
Moffett Field, California 94035

July 1976

1. Report No.	2. Government Accession No.	3. Recipient's Catalog No.
TM X-73,157		

4. Title and Subtitle	5. Report Date
AN EXPERIMENTAL AND COMPUTATIONAL INVESTIGATION OF THE FLOW FIELD ABOUT A TRANSONIC AIRFOIL IN SUPERCRITICAL FLOW WITH TURBULENT BOUNDARY-LAYER SEPARATION	6. Performing Organization Code

7. Author(s)	8. Performing Organization Report No.
Morris W. Rubesin, Arthur F. Okuno, Lionel L. Levy, Jr., John B. McDevitt, and H. Lee Seegmiller	A-6690
	10. Work Unit No. 506-26-22
9. Performing Organization Name and Address	11. Contract or Grant No.
Ames Research Center, NASA Moffett Field, Calif. 94035	
	13. Type of Report and Period Covered
12. Sponsoring Agency Name and Address	Technical Memorandum
National Aeronautics and Space Administration Washington, D.C. 20546	14. Sponsoring Agency Code

15. Supplementary Notes

16. Abstract

A combined experimental and computational research program for testing and guiding turbulence modeling within regions of separation induced by shock waves incident on turbulent boundary layers is described. Specifically, studies are made of the separated flow over the rear portion of an 18%-thick circular-arc airfoil at zero angle of attack in high Reynolds number supercritical flow. The measurements include distributions of surface static pressure and local skin friction. The instruments employed include high-frequency response pressure cells and a large array of surface hot-wire skin-friction gages. Computations at the experimental flow conditions are made using time-dependent solutions of ensemble-averaged Navier-Stokes equations, plus additional equations for the turbulence modeling.

17. Key Words (Suggested by Author(s))	18. Distribution Statement
Transonic turbulent boundary layers and skin friction	Unlimited STAR Category - 34

19. Security Classif. (of this report)	20. Security Classif. (of this page)	21. No. of Pages	22. Price*
Unclassified	Unclassified	12	$3.25

*For sale by the National Technical Information Service, Springfield, Virginia 22161

AN EXPERIMENTAL AND COMPUTATIONAL INVESTIGATION OF THE FLOW FIELD ABOUT A TRANSONIC AIRFOIL IN SUPERCRITICAL FLOW WITH TURBULENT BOUNDARY-LAYER SEPARATION

Morris W. Rubesin,* Arthur F. Okuno,** Lionel L. Levy, Jr.,**
John B. McDevitt,** and H. Lee Seegmiller**
Ames Research Center, NASA, Moffett Field, California 94035

Abstract

A combined experimental and computational research program for testing and guiding turbulence modeling within regions of separation induced by shock waves incident on turbulent boundary layers is described. Specifically, studies are made of the separated flow over the rear portion of an 18%-thick circular-arc airfoil at zero angle of attack in high Reynolds number supercritical flow. The measurements include distributions of surface static pressure and local skin friction. The instruments employed include high-frequency response pressure cells and a large array of surface hot-wire skin-friction gages. Computations at the experimental flow conditions are made using time-dependent solutions of ensemble-averaged Navier-Stokes equations, plus additional equations for the turbulence modeling.

Nomenclature

A = van Driest damping length

C_p = pressure coefficient, $(p_w - p_\infty)/q_\infty$

c = airfoil chord length

c_f = local skin-friction coefficient based on the free-stream dynamic pressure

I = wire-gage current

k = roughness height

ℓ = mixing length of turbulence

M_∞ = free-stream Mach number

Pr = Prandtl number

p_w = local surface pressure

p_∞ = free-stream pressure

q_∞ = free-stream dynamic pressure, $(1/2)\rho_\infty u_\infty^2$

R = resistance of wire gage

$Re_{c,\infty}$ = Reynolds number, $u_\infty c/\nu_\infty$

Re_θ = Reynolds number based on boundary-layer momentum thickness

R_o = resistance of wire gage at 0°C

u = local velocity parallel to chord

u_δ = velocity at edge of viscous region

u_∞ = free-stream velocity

v = local velocity normal to chord

x = distance along chord from leading edge

Δx = effective length of skin-friction gage

y = distance from surface normal to chord

y_{DS} = location of separation streamline

δ = thickness of viscous region

δ_i^* = incompressible displacement thickness (Eq. (5))

ε = eddy diffusivity

μ_w = viscosity at the airfoil surface

ν_∞ = kinematic viscosity in the free stream

ρ_∞ = free-stream density

ρ_w = density at the airfoil surface

τ_w = surface shear stress

τ_{wo} = surface shear stress on surface with constant pressure

Introduction

An understanding of the fluid-dynamic mechanisms controlling the separation of boundary layers from aerodynamic surfaces is of major importance in aeronautics. The forces and moments on aerodynamic bodies at angle of attack and the performance of diffusers within wind tunnels or aircraft engines are often governed by the existence and location of separation. Thus, the prediction of the position of the onset, the behavior of the boundary-layer separation, and the reattachment processes have occupied the fluid mechanics community for many years (e.g., Ref. 1). Until recently, however, the techniques of predicting separation have been quite approximate, at best involving iteration between essentially inviscid and viscous regions of the flow field.[2] In this iteration process the viscous region is tightly coupled to the inviscid region, whereas the reverse is not true. This unequal sensitivity had led to numerical difficulties, and the iterative process is not generally successful.

Recent developments in computer technology and numerical analysis, however, have made it possible to avoid this iterative process by permitting the time-dependent solution of the full Navier-Stokes equations for the entire flow field.[3] For two-dimensional laminar boundary layers, these solutions have been found to be quite accurate.[4] When attention is turned toward turbulent boundary layers with eddy viscosity representations of the Reynolds stress terms in the ensemble-averaged Navier-Stokes equations, it is found that these empirical methods, so useful for equilibrium boundary layers, do not work well when separation occurs.[5,6]

*Senior Staff Scientist.
**Research Scientist.

In an effort to improve turbulence modeling for boundary layers separating at sonic flight speeds, the Ames Research Center has initiated concomitant programs in experimental and numerical fluid dynamics in which the experimental results are used to help guide the development of turbulence models.

The first part of this program was reported in Ref. 7. The experiment involved the measurement of the static pressure distribution over the surface of an 18%-thick circular-arc airfoil in the free-stream Mach number range from 0.71 to 0.79 for a range of Reynolds numbers. These measurements were supplemented by flow visualization with surface oil streaks and shadowgraphs. The airfoil was tested in the Ames High Reynolds Number Channel, a facility that has top and bottom walls contoured to the shape of the streamlines computed to exist one-half the channel height away from the chordline of the airfoil in an inviscid flow for a specified design Mach number. The Reynolds numbers employed in the experiment were as high as 17×10^6, based on free-stream flow conditions and the chord length. At the highest Mach number tested, the standing shock waves on the airfoil only extended two-thirds of the distance to the contoured walls so that wind-tunnel blockage was not a factor in these experiments. In parallel with the experiments, computations of the flow field about the airfoil were performed through time-dependent solutions of ensemble-averaged compressible Navier-Stokes equations in finite-difference form.[8,9] The turbulence models used in these calculations included the usual algebraic formulations for eddy viscosity,[10] which imply the turbulence is in equilibrium with the mean flow, and semi-empirical turbulence lag models that attempt to account for turbulence history. In addition, some unique eddy viscosity formulations were required in the separated region downstream of strong standing shock waves; these are presented in the present paper in the section devoted to the flow-field computations.

In Ref. 7 detailed comparisons were made between the measured and computed surface pressure distributions for two Mach numbers at a chord Reynolds number of 4×10^6. In either case, a standing shock wave terminates the supercritical flow, that is, the supersonic flow region that develops adjacent to the airfoil. At $M_\infty = 0.74$, the standing shock wave is too weak to separate the boundary layer, and separation only occurs very close to the trailing edge where the pressure rises quite rapidly. The computations, with the different eddy viscosity models of turbulence, predicted shock-wave locations about 5-10% of the chord downstream of the actual location. Modifications of the turbulence model that improved the prediction of the shock-wave location resulted in too low a pressure recovery at the trailing edge. At $M_\infty = 0.79$, the standing shock wave induced separation at about $x/c = 0.675$. When the turbulence models were adjusted in an attempt to fix the standing shock wave where the experimental wave is located, the predicted pressure recovery in the separated region was much too high.

Surface pressure distributions, while contributing to an overall assessment of the accuracy of a specific turbulence model computation for a given flow condition, contain insufficient information to guide improvements necessary in the turbulence model. Traditionally, this guidance has been provided by detailed mean velocity surveys through the boundary layer (e.g., Refs. 10 through 14), with the measurements close to the surface being particularly useful. Because the current experiment involved a very small model operating at a high unit Reynolds number (80×10^6/m), the boundary layers on the model were too thin (0.4 mm) to survey with impact pressure probes, hot wires, or a laser doppler velocimeter in either the viscous sublayer or the fully turbulent wall region of the boundary layer. Further, intrusive probes, such as impact pressure probes or hot wires, together with their support mechanisms, were considered possible sources of flow interference at the transonic flow conditions of the present experiment. To avoid such interference and, yet, to gain insight into the mechanisms taking place within the boundary layer close to the surface, reliance was placed on measurements of the local skin friction.

The flush heated wire gage described in Ref. 15 was particularly suited to the task of measuring the local skin friction because of its compact configuration and insensitivity to streamwise pressure gradients that would occur on the airfoil. A design decision had to be made as to whether the individual gages would be (1) mounted on buttons that could be calibrated in channel flows and then placed in cavities on the wing surface; or (2) mounted directly on the surface of the wing and calibrated indirectly by operating the wing under conditions where boundary-layer calculations of local skin friction were expected to be accurate. The latter option was adopted as the simpler approach, and one which could yield an aerodynamically smoother surface. Thus, in effect, the gages read skin-friction values relative to those that existed on the wing at free-stream Mach numbers where the external and boundary-layer flows were believed to be understood.

Since all the instrumentation employed in the present investigation had response times of less than 0.01 sec, dynamic as well as static measurements were taken to determine if shock-induced separations that appear to be steady were really so. Thus, dynamic measurements of skin friction are presented.

Because the experiment described herein utilized the same facility reported thoroughly in Ref. 7, the experimental emphasis here will be on the skin-friction model. For completeness, the turbulence model used in the calculations presented in this report is given in detail because it forms the basis for some discussion of the results. Finally, the dynamic behavior of the surface measurements is discussed.

Experimental Procedures

Ames High Reynolds Number Test Channel

The Ames High Reynolds Number Test Channel was used for the skin-friction experiments described. The channel consists of a large high-pressure air supply, a test section, and a large-volume vacuum vessel, described in detail in Ref. 7. A schematic diagram of the test section of the channel is shown in Fig. 1. The air enters the test section through a bellmouth, passes through the test section and a speed control region before entering the diffuser that leads to the vacuum vessels. For the current experiment, the pressure distribution and skin-friction airfoil models spanned the test section and were mounted from the side walls. The upper and lower test section walls were contoured as described in the previous section. In addition to the

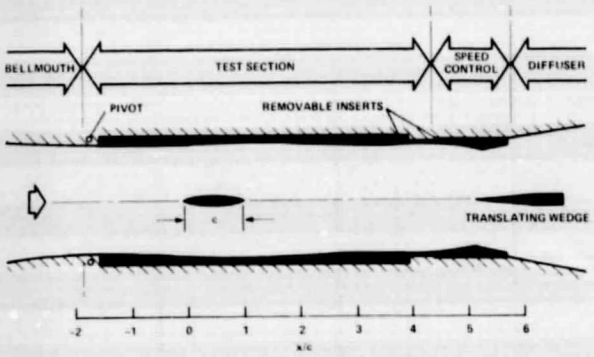

Fig. 1 Schematic diagram of Ames High Reynolds Number Test Channel

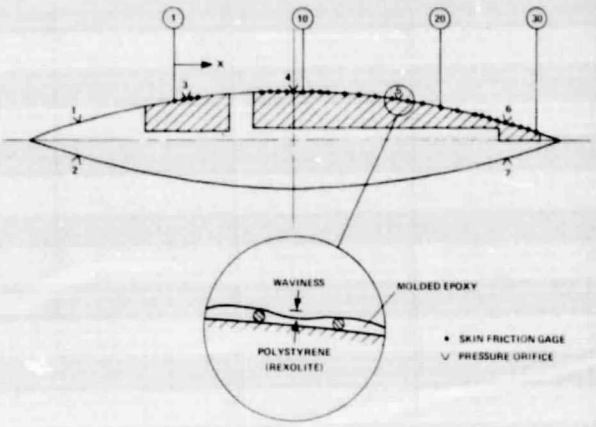

Fig. 2 Skin-friction model instrumentation

contouring, the upper and lower walls of the test section could be pivoted about their leading edges to permit compensation for the displacement effects created by the boundary-layer growth on the four walls of the test section. The Mach number in the channel was controlled by adjusting the flow area in the speed control section with inserts in the top and bottom walls and by translating a wedge axially along the test section centerline.

The air and vacuum supplies of the Ames High Reynolds Number Channel are adequate to permit operation at a relatively high unit Reynolds number of 85×10^6/m for a maximum period of 45 sec. During this time interval, Joule-Thompson cooling of the air supply causes the stagnation temperature of the facility to drop by about 10°C.

Experimental Models

Two models having identical external configurations were utilized in the experiment. Each is a circular-arc airfoil, 18% thick, with a chord length of 0.2032 m. The first model, designed for measurements of the pressure distribution about the model, was made of steel with a surface finish of 0.000813 mm. The model contained 47 pressure taps on one surface and 3 on the other side to allow aligning the airfoil to an angle of attack of 0°. Details of this model and of the pressure distribution experiment are given in Ref. 7. The second model, used for this skin-friction experiment, contained 7 pressure taps in addition to an array of 30 hot-wire skin-friction gages set into blocks of plastic. The purpose of the pressure taps was to ensure an alignment of the model to a 0° angle of attack and to verify that the pressure distribution on the skin-friction model, at a few discrete stations, agreed with the pressure measurements at the same stations obtained on the pressure distribution model for the same free-stream conditions and top and bottom test section wall settings. Although the models spanned the test section of the channel, the flow field in the vicinity of the center span of the model away from the side-wall boundary layers was found to be two-dimensional, even under conditions where large regions of separation occurred over the airfoil and on the side walls.[7]

The schematic drawing of the skin-friction model, presented in Fig. 2, shows the sections of two rather large cavities in the model (shaded areas) containing polystyrene plastic (rexolite) that was molded into place and which supports the lead-in wires and the skin-friction gage wire elements.

Table 1 Location of skin-friction gages

Wire no.	x/c	Wire no.	x/c	Pressure orifices	x/c
1	0.276	16	0.651	1,2	0.1
2	0.292	17	0.676	3	0.3
3	0.308	18	0.713	4	0.5
4	0.324	19	0.744	5	0.7
5	0.437	20	0.775	6,7	0.9
6	0.453	21	0.805		
7	0.469	22	0.821		
8	0.484	23	0.836		
9	0.500	24	0.851		
10	0.516	25	0.866		
11	0.531	26	0.881		
12	0.547	27	0.896		
13	0.562	28	0.911		
14	0.589	29	0.926		
15	0.621	30	0.941		

Photographs of the model are shown in Figs. 3 and 4. The dull spanwise streaks are filled cavities that contain tubes leading to the pressure taps. The wires composing the skin-friction gages were placed on the surface of the plastic inserts in a direction normal to the stream between pairs of lead-in posts, and epoxy plastic was molded in between the wires as shown in the inset on Fig. 2. This technique for construction of the skin-friction gages is identical with that developed in Ref. 15. On the current model the gage wires were made of platinum having a diameter of 0.0254 mm and lengths in the spanwise direction of about 6.35 mm. One problem with this type of model construction is the maintenance of an aerodynamically smooth surface at the joints between the polystyrene and steel, and in the epoxy between the individual wire gages. Because of the relative softness of the plastic surfaces and the rather delicate nature of the wire gages, it was decided to make surface contour measurements without actually touching the surface. A low-intensity, but narrow laser light beam was projected on the surface of the model and the position of the reflection was noted on a screen across the laboratory. The local surface angle of the model was determined from the geometric arrangement of the laser, model, and screen. From these measurements it was a simple matter to deduce surface waviness or roughness heights of about 0.0004 mm. It was found that the model had a waviness of less than 0.004 mm in an average distance of 3.18 mm between the wire gages (see inset in Fig. 2). The step heights in the

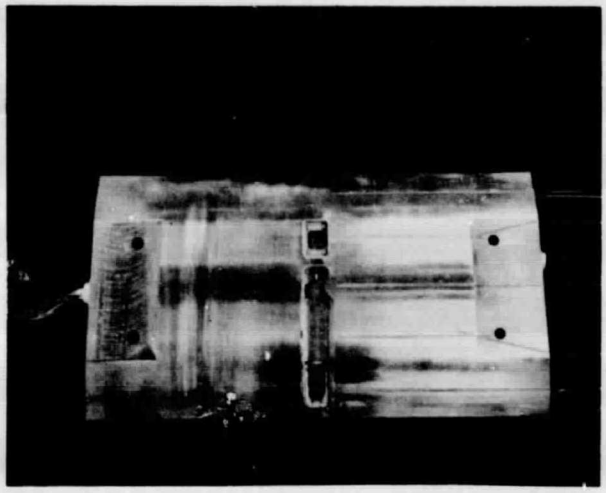

Fig. 3 Photograph of skin friction model.

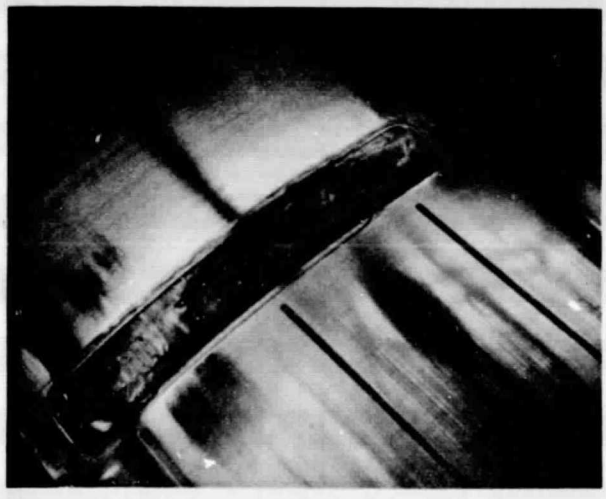

Fig. 4 Detailed photograph of skin friction model showing lead-in posts and gage wires.

surfaces where the plastic and steel met were less than 0.0003 mm. For reference, the criterion for aerodynamic smoothness in an attached boundary layer is $\sqrt{c_f/2}\,(u_\infty k/\nu_\infty) < 5$, where k is the allowable surface roughness height.[1] In the regions of attached flow for the conditions of this experiment, the values of k are about 0.0023 mm or one-half the actual surface waviness. It can be expected, from the data summarized in Ref. 1, that the surface waviness on the skin-friction model could cause the measured skin friction to be about 5% high in the regions of attached flow. For separated regions, the surface waviness should be less influential. These are acceptable errors for an heuristic experiment such as this.

For future reference, the numbering and corresponding positions of the skin-friction gages are shown graphically in Fig. 2 and are also given in Table 1.

The buried-wire skin-friction gages used in this experiment are still in the development stage; therefore, their calibration was conducted as an intimate part of the main experiment. Details of the calibration procedure and related discussion are given in the results section.

Computational Method

The computations of the flow field about the airfoil at $M_\infty = 0.788$, where boundary-layer separation is induced by the shock wave, were performed using a form of the computer program described in Ref. 9. The computer program utilizes an explicit finite-difference method to solve the time-dependent, two-dimensional ensemble-averaged Navier-Stokes equations applicable to compressible turbulent flows. The turbulence is modeled with an algebraically expressed eddy diffusivity model, termed Model 3 in Ref. 9. This model assumes that the turbulence is in equilibrium with the local mean flow. With reference to the following sketch, the eddy diffusivity expressions for the various regions indicated are as follows:

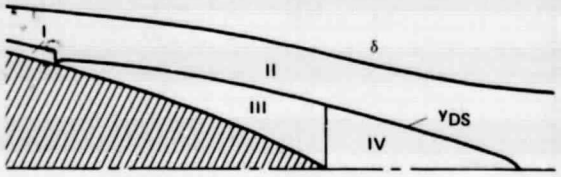

Inner region I

$$\varepsilon = \ell^2\left[\left(\frac{\partial u}{\partial y}\right)^2 + \left(\frac{\partial v}{\partial x}\right)^2\right]^{1/2} \tag{1}$$

$$\ell = 0.41y(1 - \exp(-y/A)) \tag{2}$$

where

$$A = 26\,\frac{\mu_w}{\rho_w}\sqrt{\rho_w/|\tau_w|} \tag{3}$$

This is essentially the classical van Driest model for the inner portion of a turbulent boundary layer. The term $\partial v/\partial x$ has been added to Eq. (1) to account for departures from true boundary-layer flow as the point of separation is approached. The van Driest damping length A is expressed identically as on a flat plate, with no account being made for the effect of surface pressure gradients as is suggested, for example, in Ref. 10.

II Outer region of boundary layer and wake

$$\varepsilon = \frac{0.0168u_\delta\delta_i^*}{1 - [(y - y_{DS})/\delta]^6} \tag{4}$$

where y_{DS} is the location of the streamline boundary of the separated region and δ is the overall thickness of the viscous region. The displacement thickness δ_i^* is defined as

$$\delta_i^* = \int_{y_{DS}}^{\delta}(1 - u/u_\delta)dy \tag{5}$$

Equation (4) is based on the Clauser model,[12] but accounts for intermittency of the turbulence in the wake with the term containing y. The usual definition of δ_i^* is modified with the lower limit of integration moved from the surface to the separation streamline y_{DS}.

III Separation bubble wall region

$$\varepsilon = 0.0168 u_\delta \delta_i^* \{(y/y_{DS})[1 - \exp(-y/\Lambda)]\}^2 \qquad (6)$$

IV Separation bubble wake region

$$\varepsilon = 0.0168 u_\delta \delta_i^* \qquad (7)$$

Discussion of Results

Surface Pressure Distribution

The transonic flow over the circular-arc, 18%-thick airfoil was studied in Ref. 7 with the pressure distribution model for a rather extensive range of Mach and Reynolds numbers. In these experiments, the upper and lower walls of the channel were contoured to conform to the free streamlines that would exist over this airfoil for free flight in an inviscid fluid at $M_\infty = 0.775$. The channel walls and their positioning were kept constant for all the Mach and Reynolds numbers of the tests. Mach number was controlled by adjusting the dimensions of a downstream nozzle throat and the position of the translating wedge (see Fig. 1). The Reynolds number was controlled by setting the stagnation pressure. The stagnation temperature is uncontrolled, but remained close to ambient and was continuously monitored. Supercritical flow, where the local velocity at the surface of the airfoil exceeds the local sonic velocity, was found to occur above $M_\infty = 0.71$. Between $M_\infty = 0.76$ and 0.78, an unsteady, asymmetric periodic flow occurred. At Mach numbers below the unsteady flow regime the boundary layer remained attached until the trailing edge was approached; in the unsteady regime, separation alternately switched from the trailing edge to the base of the shock wave; and above $M = 0.78$ separation was fixed at the base of the shock wave.

Since the objective of the present experiment was to define the local skin friction for the case of nominally steady shock-induced separation, it was necessary to test at a Mach number greater than 0.78. Thus, the skin-friction experiments were conducted at $M_\infty = 0.783$ for chord Reynolds numbers ranging from 8×10^6 to 14.3×10^6. For calibration of the skin-friction gages, the skin-friction model was also run at $M_\infty = 0.682$ where the flow is subcritical and boundary-layer theory can be expected to apply over almost all of the airfoil with reasonable accuracy. Because the Mach numbers employed in these tests differ from that used to design the contours of the upper and lower walls, and also because viscous effects including the rather large separation zones would also cause the actual streamlines away from the airfoil to deviate from those based on inviscid theory, it cannot be expected that the pressure and skin-friction distributions measured in this experiment would conform closely to free-flight conditions. It would be expected, however, that the behavior in the two types of flows, that is, in the specific channel configuration and in free flight, would be sufficiently similar so that the separation mechanisms studied in one flow field would be representative of the other. In the channel, strict application of the computational method for calculating the turbulence separation on the airfoil requires introduction of the actual upper and lower wall contours as boundary conditions in the computer program. This is being done at present; however, the computer results given in this paper were based on free-flight conditions and when comparing the data and the computations this innate difference must be considered before drawing conclusions.

Representative surface-pressure distributions on the airfoil for the two test Mach numbers of this experiment are shown on Fig. 5. The ordinate is the pressure coefficient C_p and the abscissa is the station represented as a fraction of the chord. The data for $M_\infty = 0.784$ and $Re_{c,\infty} = 10.7 \times 10^6$ indicate shock-induced separation occurred at about $x/c = 0.675$. Beyond this station the pressure recovery is quite poor. The pressure measurements on the skin-friction model (filled symbols) show that the flow conditions over the two models could be reproduced quite well. The subcritical case is represented by the data at $M_\infty = 0.682$ and $Re_{c,\infty} = 12.4 \times 10^6$. At this Mach number, significant pressure recovery occurs toward the trailing edge. Again, there is good agreement between the pressures measured on the pressure distribution and skin-friction models (open and filled symbols, respectively). The data obtained at other Reynolds numbers ($3.1 \times 10^6 \le Re_{c,\infty} \le 14.3 \times 10^6$) are quite similar to those shown in Fig. 5. The positions of separation indicated on the figure for the two test cases were determined from oil-film photographs.[7]

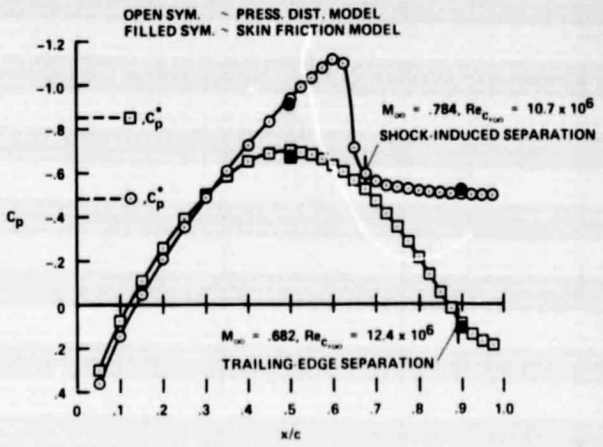

Fig. 5 Pressure distributions on airfoil for trailing-edge and shock-induced separation

Calibration of Skin-Friction Gages

The principle of the heated wire skin-friction gage requires that its dimension in the streamwise direction be small compared to the boundary-layer thickness. As the effective dimension of the gage is composed of the actual diameter of the heated wire plus the region of the substrate surface whose temperature is elevated because of the heat conducted upstream from the wire, it is necessary for the gage wire diameter to be very fine and for the substrate to have a very low thermal conductivity (Refs. 15 and 16). When these conditions are met, the heat transferred from the heated wire element forms a thermal boundary layer over the gage that lies within the viscous sublayer immediately adjacent to the surface. Because the flow here is

essentially laminar, the heat-transfer mechanisms are governed by the fluid properties and the velocity gradient normal to the surface, or skin friction, that exists just upstream of the gage. Thus, the power lost from the gage, per unit of temperature rise over the unheated airfoil surface at the same station, becomes a measure of the local skin friction.

The measurements of skin friction are sensitive to the local surface-pressure gradients as was shown in Refs. 15 and 17. Equation (5) of Ref. 15 contained a typographical error of one order of magnitude for the pressure gradient term. To correct that error, and to put the equation for pressure gradient effects into a form useful for the present experiment, the effect of pressure gradient is expressed as

$$\frac{\tau_w}{\tau_{wo}} = 1 - 0.312\left[\frac{(\Delta x/c)}{(c_f/2)Re^2_{c,\infty}Pr}\right]^{1/3}\frac{1}{c_f}\frac{dC_p}{d(x/c)} \qquad (8)$$

where τ_w is the actual shear and τ_{wo} is the shear induced from the gage when the effects of surface pressure gradients are neglected. Incidentally, when the equations of Ref. 17 were put in the form of Eq. (8), the constant in the pressure gradient term was 0.344.

Equation (8) shows that a smaller Δx tends to reduce the effect of nonzero pressure gradients, though the effect of Δx is only to the 1/3 power. It also shows that at separation, where $c_f \to 0$, pressure gradients dominate the value of the skin friction. To estimate the effects of pressure gradients in the present experiment, Eq. (8) was applied to two portions of the airfoil. At $M = 0.784$, Eq. (8) was evaluated at $x/c = 0.64$, the location of the foot of the shock wave. With estimated values of $c_f = 0.003$ and $\Delta x = 3 \times$ (wire diameter),[15] it was found that the resulting τ_w was 3.2% lower than τ_{wo}, the value of shear stress that would be interpreted to exist when the effects of pressure gradient are ignored. In the region after separation, the pressure gradient was much lower, but skin friction magnitudes were also expected to be lower, for example, $c_f = 0.0003$. Here errors introduced by neglecting the effects of pressure gradient were about 0.7%. These estimated errors were sufficiently small to lead to the decision to neglect surface-pressure gradient effects in the data reduction.

The first step in calibrating the skin-friction gages was to determine their electrical resistance as a function of temperature. This is needed in order to use the gages as resistance elements as well as heater elements. This step was accomplished by placing the skin-friction model in an environmental test chamber capable of maintaining temperatures between -130° and 300°C. Two thermocouples were located on the plastic insert, one on the steel airfoil, and one in the air just above the plastic insert. A small fan inside the chamber circulated the air to minimize temperature gradients. As a consequence, the thermocouples showed departures from their mean temperature reading of only about 0.06°C. The resistances of the wires were read and recorded on the channel instrumentation system (electronic millivoltmeter plus magnetic tape recorders) so that the calibrations and application of the gages used the same read-out equipment.

The results of the electrical resistance calibration of the 30 skin-friction gages are shown on Fig. 6. For comparison, the resistance of a free

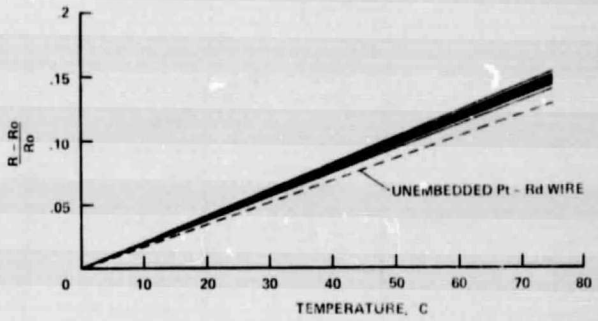

Fig. 6 Temperature dependence of the electrical resistance of the skin-friction gages

wire loop of the same platinum wire used for the gages is also shown. The reference temperature was chosen to be 0°C, and measurements were made up to 75°C. It is observed that the wire gages mounted on the airfoil model showed greater changes of resistance with temperature than did the free wire. This is explained by the stretching of the mounted wires resulting from the polystyrene having a larger linear thermal expansion coefficient (7×10^{-5}/°C) than does the platinum (0.89×10^{-5}/°C). Although the wires gave individual readings of resistance change within about 1% of each other, the individual wire calibrations were used in the data reduction to account for the small differences in resistance that existed between the wires, and which could cause temperature differences of a few degrees if a single mean curve were used.

The skin-friction model was then mounted in the Ames High Reynolds Number Channel and the gage wires were electrically connected to be used either as resistance elements, for surface temperature measurements, or to be driven by standard constant temperature mode hot-wire equipment, where the instantaneous voltage required to maintain a preassigned overheat is measured and recorded. As six DISA systems were available, only six wires were heated during any given run. This was not a serious limitation because it was shown in Ref. 15 that heating a gage immediately upstream of another gage could affect the latter's readings. For the measurement of the magnitude of skin friction, several wires were left unheated between the heated skin-friction gages to minimize the interference. This interference effect, in fact, is the basis of the separation detector explained in Ref. 15 and was used in the present experiment to define the sign of the skin-friction measurements in the separated zones. Unheated wires downwind of a heated gage indicated temperatures in excess of what would have been expected at that location in the absence of heating.

As stated earlier, boundary-layer computations, under conditions where boundary-layer theory is expected to give good indications of the skin friction, were used to "calibrate" the skin-friction gages. To gain some insight into the accuracy of this process, two different boundary-layer programs containing different turbulence models were compared for the subcritical pressure distribution ($M_\infty = 0.682$) shown on Fig. 5.

One program, called Marvin-Sheaffer, is an extension of Ref. 18 that contains a two-layer algebraic eddy viscosity model similar to that of Ref. 10 and, thereby, assumes that the turbulence is

always in equilibrium with the mean flow. The second computer program allows for departures from equilibrium between the turbulence and the mean flow by introducing two differential equations for the intensity and scale of the turbulence.[19] This latter program is an extension of the work of Saffman[20] and, for reference, is called the Modified Saffman model. In its present form, it can also account for the streamline curvature along the surface of the airfoil as an option.

The distributions of skin friction that resulted from applying these programs to the airfoil with a pressure distribution corresponding to $M_\infty = 0.682$, Fig. 5, are shown in Fig. 7 for the case where the channel was operated at a total pressure of 60 psia. The Marvin-Sheaffer program required the positions of the beginning and the end of transition to turbulence to be specified. The transition locations were

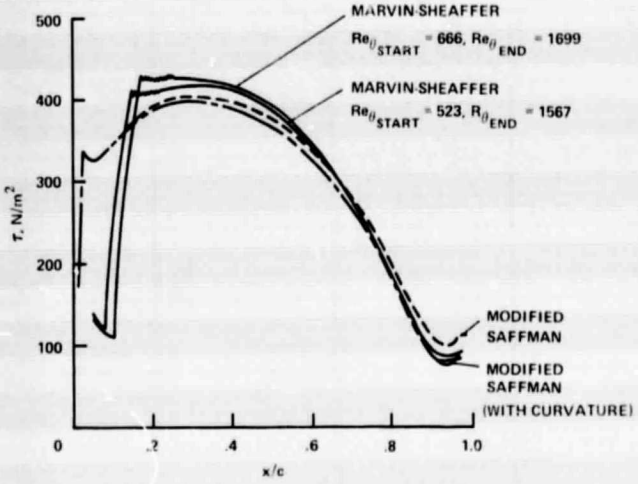

Fig. 7 Calculated skin friction on airfoil for conditions of an attached boundary layer, $M_\infty = 0.682$, $Re_{c,\infty} = 12.4 \times 10^6$

estimated from plots of the power lost per unit temperature rise, $I^2R/\Delta T$, recorded by the skin-friction gages. The location where the $I^2R/\Delta T$ began rising rapidly with distance along the chord was chosen as the point of onset of transition. The location of the end of transition was taken where the $I^2R/\Delta T$ reached a first maximum. When the skin-friction gage data at the four different stagnation pressures or Reynolds numbers were examined in this way, it was noted that transition onset could be represented reasonably well by a value of $Re_\theta = 523$ and the end of transition by $Re_\theta = 1567$. Of course, not all the data agreed exactly with these criteria but the data could be bounded, for example, on the high side by $Re_\theta = 666$ and $Re_\theta = 1699$ for the onset and end of transition, respectively. The results from the Marvin-Sheaffer program based on both sets of transition criteria indicate in Fig. 7 that skin friction downstream of transition is relatively insensitive to small changes in transition location. At the trailing edge the two calculations differ by about 10%, but it is not clear why differences caused by the location of transition near the leading edge of the airfoil would be largest farthest downstream from transition.

To show how sensitive the predicted skin friction is to the particular model of turbulence employed in the calculations, computations based on the Modified Saffman model are also shown on Fig. 7. Because the earlier Marvin-Sheaffer computations did not show much sensitivity to the transition locations, no particular care was taken to match the transition to the data. Transition was arbitrarily initiated at $x/c = 0.02$ and allowed to run its course within the computer program. One Modified Saffman curve includes the effect of the convex surface curvature of the airfoil whereas the other treats the airfoil boundary layer as one on a flat plate experiencing the pressure distribution occurring on the airfoil. A comparison of these two curves indicates that the effect of the convex surface curvature is to reduce the local skin friction by an amount that increases with distance along the airfoil surface, or more directly, the boundary-layer thickness. At the trailing edge, where the boundary layer is the thickest, the difference caused by the curvature is about 30% of the relatively small values of shear occurring there. At $x/c = 0.7$, the curvature effect is only about 5%.

From the curves shown in Fig. 7, it is observed that beyond $x/c = 0.3$, the region of interest in the separated flow test, the results of the Marvin-Sheaffer program and the Modified Saffman program with surface curvature agree to within 10%. Thus, either program could be used for "calibrating" the skin-friction gages; because the Marvin-Sheaffer program runs very quickly, it was used for evaluating the shear on the airfoil for channel total pressures of 15, 30, and 45 psia, in addition to the 60 psia values shown in the figure.

The skin-friction gage calibration process consisted of testing the airfoil at $M_\infty = 0.682$ at a series of Reynolds numbers. During each test, six widely separated skin-friction gages were heated and the power loss per unit of temperature rise ($I^2R/\Delta T$) within each heated gage was determined. The temperature of the heated gages and of those unheated wires measuring the airfoil surface temperature just upstream of the heated gages (i.e., the ΔT) were determined from the electrical resistance R measured for each wire and from the curves of Fig. 6.

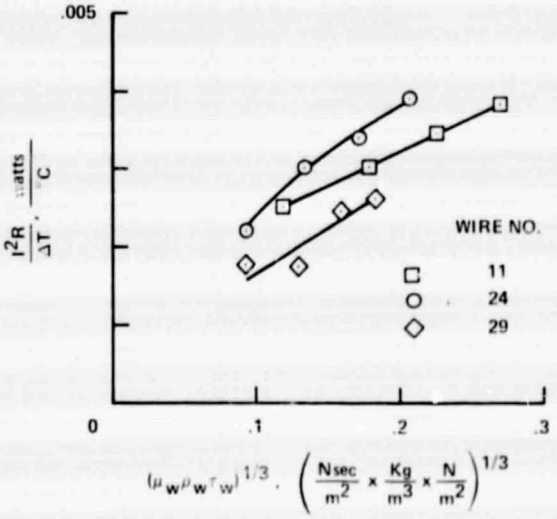

Fig. 8 Calibration curves of representative skin-friction gages

For each successive run, another series of six gages was heated, and so on until all the gages were heated for a given Reynolds number. Five runs were needed at each Reynolds number to cover the 30 gages on the model and a sixth run was made to measure the airfoil surface temperature without heating any of the wires. This process was repeated for the four Reynolds numbers. When the measured power loss per unit of temperature rise for each gage was plotted against the calculated values of $(\mu_w \rho_w \tau_w)^{1/3}$ for the corresponding test conditions and gage locations, curves such as those in Fig. 8 resulted. Note that $(\mu_w \rho_w \tau_w)^{1/3}$ is used as the abscissa in this figure because the basic theory underlying the gages shows the power loss per unit temperature rise to be linearly proportional to this quantity. The range of the representative curves shown on Fig. 8 encompasses all the gages and provides an indication of the maximum variation between the gages. At the lower values of shear, conduction effects in the plastic substrate cause a departure from linearity (see the curve for wire 24), and this had to be accounted for in the calibration, especially since low values of shear were expected in the region of separated flow.

Comparison of Computed and Measured Flow Field

In this section, comparisons will be made of the computed and measured flow-field characteristics for $M_\infty = 0.788$, where shock-induced boundary-layer separation occurs. In considering these comparisons, it must be recalled that the computations at this time apply only to free-flight conditions and may not closely agree with calculations employing identical turbulence models but utilizing the contours of the upper and lower walls of the channel as boundary conditions. The comparisons, then, of the numerical solutions and the data must be viewed in a qualitative sense.

In Fig. 9, the calculated and measured surface pressure distributions are compared. From experience with inviscid flow-field computations, it is felt that the mismatch in the location of the shock wave shown in this figure is due in part to the differences between the boundary conditions of the calculations and those that actually existed in the channel with contoured walls designed for $M_\infty = 0.775$. Of course, the turbulence modeling also has a large effect on the shock-wave location. The small Mach and Reynolds number differences between the calculations and the experimental conditions, however, are believed to be insignificant. This judgment is based on a comparison of a series of computed results with a specific turbulence model and free-flight boundary conditions for a range of Mach and Reynolds numbers.[9] A qualitative conclusion of the comparison between the data and computations in Fig. 9 is that the turbulence model employed in the present calculations (see Computational Method) results in too high a pressure recovery. Physically, this would imply that the predicted thickness of the separated region is too narrow. An eddy diffusivity that is too large overall could cause the narrow separation region.[9] For turbulence in equilibrium with the mean flow, there is a contradiction here in that thinner regions of viscous flow usually result in smaller values of eddy diffusivity in the outer regions since $\varepsilon \sim \delta^*$. This implies that the chief turbulence modeling difficulties lie with the modeling of the inner regions, regions I and III of the sketch in the section on Computational Method. An alternative means of achieving lower effective eddy diffusivities in the modeling involves use of the concept of turbulence lag (e.g., Refs. 4 and 9).

Figure 10 shows the distribution of the local shear stress coefficients, based on the free-stream dynamic pressure, that were obtained from the skin-friction gages at $Re_c = 10.7 \times 10^6$ and 14.3×10^6. For values of x/c less than 0.675, that is, ahead of separation, predictions could be based on the Marvin-Sheaffer boundary-layer program and the experimental pressure distributions. The difference between these lines is an indication of the magnitude of the effect Reynolds number has on the local skin-friction coefficient for the attached flow.

The data obtained with the skin-friction gages are shown in Fig. 10 for $Re_c = 14.3 \times 10^6$ and for $Re_c = 10.7 \times 10^6$. It is noted that many of the wire

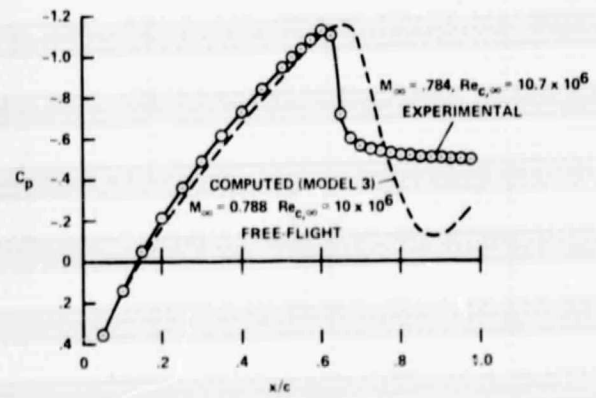

Fig. 9 Comparison of experimental and computed pressure distribution on airfoil with shock-induced separation

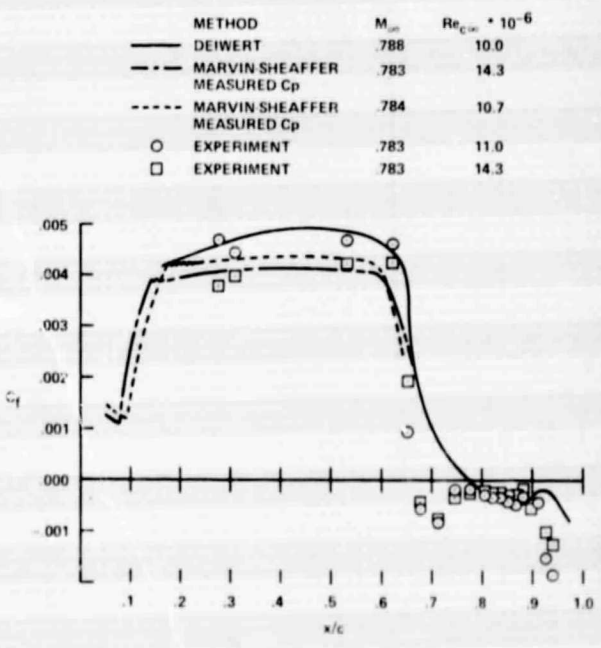

Fig. 10 Distribution of skin-friction coefficient in the presence of boundary-layer separation

gages indicated on Fig. 2 and in Table 1 are not represented on Fig. 10. The reason for this is that after calibration several of the gages broke during the running of the experiment. The gage wires are extremely delicate and were damaged by particles of dirt in the air that were accidentally introduced into the channel. Fortunately, the damaged wires were limited to values of x/c less than 0.5. Usually, the wires were damaged by being broken or pulled away from their lead-in posts. A few wires were completely pulled off the model. Visual examination of the broken wires before and after runs indicated that no fragments of wire extended into the airflow to cause major disturbances. Fortunately, the objectives of the present experiment were identified with processes taking place aft of the x/c = 0.5 station, where none of the wires was broken. The increased surface roughness probably introduced by the upstream broken wires is not expected to have affected the results beyond x/c = 0.675 because of the rather thick viscous layers there and the relatively long distance between the last of the broken wires and the region of gages that remained intact.

A comparison of the experimental data at x/c = 0.276, 0.308, and 0.531, where the flow is attached, with the Marvin-Sheaffer calculations (identical with those used to "calibrate" the wire gages) is an indication of the repeatability of the skin-friction measurements. These points are all within 10% of the boundary-layer computations corresponding to the appropriate Reynolds number and experimental pressure distribution. If the repeatability is taken as a measure of the uncertainty of the measurement and if the percentage uncertainty in the power measurement is treated as constant, the uncertainty in skin friction at the low values in the separated region is estimated to be about 15%. The uncertainty in the region of separated flow and low skin friction is larger because the heat transferred to the substrate material of the heated wire gage becomes proportionately larger.

The solid line represents the values of the skin-friction coefficient obtained from Deiwert's Navier-Stokes code and the turbulence modeling described previously for a Reynolds number of 10×10^6, and is to be compared with the experimental data represented by circles. Again, because of the difference in boundary conditions between the free-flight computations and those that existed in the channel, only qualitative comparisons are meaningful. As with the pressure distributions, the predicted skin-friction coefficient does not drop at quite the same chordwise station as the data. The predicted values indicate the shock-wave location at a larger x/c than the data, which is generally consistent with the pressure distribution results; however, the difference in shock location indicated by the skin-friction data is somewhat less than in the case of the pressure data.

In general, the experimental data and the computations show a similar character in the separated flow region. After separation, a maximum shear in the negative direction develops. This shear diminishes in magnitude with distance back on the airfoil for a while, and then approaches a second maximum in the absolute sense as the trailing edge is approached. This general character suggests strong flow reversal. The computations confine this behavior to a region closer to the trailing edge than is evident in the data, which is consistent with the downstream prediction of the shock-wave position. The magnitude of the reversed shears, however, are seriously underpredicted just beyond separation and near the trailing edge. Near the trailing edge this may be caused by a reversal in the pressure gradient in the computations beyond x/c = 0.9. It should be noted that beyond the airfoil the pressure gradient becomes strongly adverse again, which suggests a computational singularity at the trailing edge.

Fluctuating Skin-Friction Measurements

To gain some knowledge of the relative characteristics of skin-friction fluctuations in regions of attached and separated flows, the ac components of the output voltages of the heated wires were recorded on magnetic tape for subsequent analysis. Because the wire gages are imbedded in plastic, their frequency response is low (1200 to 1600 Hz) compared to that of a conventional hot-wire anemometer; hence, the fluctuating voltage output by the gages is in response to only some fraction of the total fluctuation in skin friction present at the airfoil surface. In order to compare the fluctuating skin friction on an equitable basis of frequency content, the recorded signal of each heated wire was passed through a 1000-Hz cutoff filter prior to evaluating its rms voltage. The rms values of $(\mu_w \rho_w \tau_w)$ were evaluated using the rms voltage output, ΔT, the resistance of each wire gage, and assuming that the power loss per unit temperature varies linearly with $(\mu_w \rho_w \tau_w)^{1/3}$ over the range of the fluctuation.

The chordwise distribution over the airfoil of the ratio of the rms-to-mean values of $(\mu_w \rho_w \tau_w)$ is shown in Fig. 11 for shock-induced separation at $M_\infty = 0.784$ and $Re_{c,\infty} = 8 \times 10^6$. Ahead of the shock wave, in the region of attached flow, the fluctuations are a small fraction of the mean value and

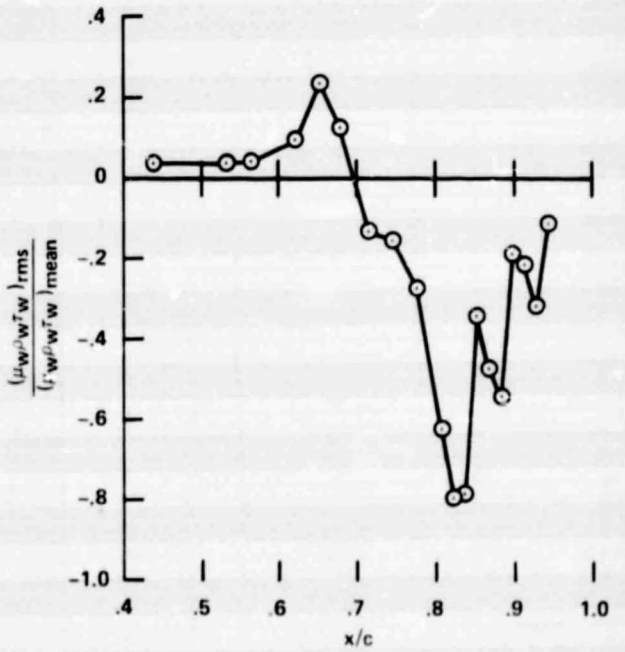

Fig. 11 Skin-friction gage fluctuations (0-1000 Hz) for shock-induced separation on the airfoil: $M_\infty = 0.784$, $Re_{c,\infty} = 8 \times 10^6$

increase downstream as the shock is approached. In the separated flow region behind the shock wave, where the mean value of τ_w is small (see Fig. 10), fluctuations in the quantity $(\mu_w \rho_w \tau_w)$ approach values that are nearly as large as the mean and, near the trailing edge, again become a small fraction thereof. The sign of the ordinate in Fig. 11 corresponds to that of τ_w in the mean value and was determined by the sign of the skin-friction coefficient in Fig. 10. It appears that the fluctuations in "skin friction" at 1000 Hz or less are a large fraction of the mean value in regions of separated flow.

Concluding Remarks

The flush hot-wire skin-friction gage has been demonstrated to be able to measure the local skin friction on a transonic airfoil experiencing shock-wave-induced turbulent-boundary-layer separation in high Reynolds number flow. The estimated accuracy of these measurements is about 15%. Together with local surface pressures measured on the same airfoil, these data provide the bases for testing and verifying computations based on Reynolds-averaged Navier-Stokes equations that are closed through turbulence modeling. To date, however, the computer codes have not progressed sufficiently to permit efficient development of a new turbulence model. One serious shortcoming of computer codes employed to date is that they apply strictly to free-flight conditions and do not accommodate test channel wall configurations. This mismatch in boundary conditions can have significant effects on the flow field immediately next to the airfoil surface. Therefore, before different turbulence models can be quantitatively tested against the pressure and skin-friction data it is necessary to incorporate the channel wall configuration and the boundary-layer displacement effects into the boundary condition of the computer codes. This is being done currently.

With the proper boundary conditions, it will be possible to test computer codes containing different kinds of turbulence models and numerical logic against the data presented here. The predicted pressures already suggest that the turbulence model used in the present calculations yields a separation region that is narrower than would be consistent with the pressure measurements. The message within the skin-friction data is less clear because the flow in the separation bubble is sensitive to modeling changes throughout the flow field and must await systematic turbulence model modifications in a code with proper boundary conditions to provide modeling guidance.

The comments above imply the belief that Reynolds stress modeling can ultimately be made to fit both the experimental pressure and skin-friction data in the separated layer. In the narrow empirical sense this is true, yet the large dynamic character of the skin-friction data found to exist in the separated zone may be incompatible with universal statistical turbulence models appropriate to other kinds of flow that are steady.

References

[1]Schlichting, H., *Boundary Layer Theory*, McGraw-Hill Book Co., 1960.

[2]Murphy, J. D., Presley, L. L., and Rose, W. C., "On the Calculation of Supersonic Separating and Reattaching Flows," SP-347, Paper 6, March 1975, pp. 151-175, NASA.

[3]MacCormack, R. W., "Numerical Solution of the Interaction of a Shock Wave with a Laminar Boundary Layer," Proceedings of the 2nd International Conference on Numerical Methods in Fluid Dynamics, *Lecture Notes in Physics*, Vol. 8, Springer-Verlag, 1971.

[4]Rose, W. C., "Practical Aspects of Using Navier-Stokes Codes for Predicting Separated Flows," AIAA Paper 76-96, 1976.

[5]Marvin, J. G., Horstman, C. C., Rubesin, M. W., Coakley, T. J., and Kussoy, M. I., "An Experimental and Numerical Investigation of Shock-Wave-Induced Turbulence Boundary-Layer Separation at Hypersonic Speeds," AGARD Conference on Flow Separation, AGARD CPP-168, 27-30 May 1975.

[6]Baldwin, B. S., and MacCormack, R. W., "Interaction of Strong Shock Wave with Turbulent Boundary Layer," Proceedings of the 4th International Conference on Numerical Methods in Fluid Dynamics, Boulder, Colorado, June 1974.

[7]McDevitt, J. B., Levy, L. L., Jr., and Deiwert, G. S., "Transonic Flow About a Thick Circular-Arc Airfoil," *AIAA Journal*, Vol. 14, No. 5, May 1976, pp. 606-613.

[8]Deiwert, G. S., "Numerical Simulation of High Reynolds Number Transonic Flow," AIAA Paper 74-603, 1974.

[9]Deiwert, G. S., "Computation of Separated Transonic Turbulent Flows," AIAA Paper 75-829, 1975.

[10]Cebeci, T., and Smith, A. M. O., *Analysis of Turbulent Boundary Layers*, Academic Press, 1974.

[11]Nikuradse, J., "Turbulente Reibungsschichten an der Platte," ed. by Zentr. wiss. Ber.-Wesen. Obtainable from R. Oldenbourg, Munich and Berlin, 1942.

[12]Clauser, F. H., "The Turbulent Boundary Layer," in *Advances in Applied Mechanics*, Vol. 4 (H. Dryden et al., eds.), Academic Press, Inc., New York, 1956.

[13]Coles, D., "The Law of the Wall in Turbulent Shear Flow," in *Sonderdruck aus 50 Jahre Grenzschichtforschung*, H. Goertler and W. Tollmien, eds., Verlang Friedr. Vieweg and Sohn, Braunschweig, Germany, 1955.

[14]Coles, D., "Law of the Wake in Turbulent Boundary Layer," *Journal of Fluid Mechanics*, Vol. 1, Pt. 2, July 1956, p. 191.

[15]Rubesin, M. W., Okuno, A. F., Mateer, G. G., and Brosh, A., "Flush-Mounted Hot-Wire Gage for Skin Friction and Separation Detection Measurements," Record of the International Congress on Instrumentation in Aerospace Simulation Facilities, IEEE Publ. 75 CHO 993-6 AES, Ottowa, Canada, Sept. 22-24, 1975.

[16]McCroskey, W. J., and Durbin, E. J., "Flow Angle and Shear Stress Measurements Using Heated Films and Wires," I. Basic Engr., Vol. 94, No. 1, pp. 46-52.

[17]Brown, G. L., "Theory and Application of Heated Films for Skin-Friction Measurement," Proceedings of the 1967 Heat Transfer and Fluid Mechanics Institute, Univ. of Calif. at San Diego, June 19-21, 1967.

[18]Marvin, J. G., and Sheaffer, Y. S., "A Method for Solving the Nonsimilar Boundary-Layer Equations Including Foreign Gas Injection," TN D-5516, Nov. 1969, NASA.

[19]Wilcox, D., and Chambers, T., "Computation of Turbulent Boundary Layers on Curved Surfaces," CR-137853, Jan. 1976, NASA.

[20]Saffman, P. G., "A Model for Inhomogeneous Turbulent Flows," *Proceedings of the Royal Society, London*, A317, 1970, pp. 417-433.